Developmental Biology 366 (2012) 172–184

Contents lists available at SciVerse ScienceDirect

Developmental Biology

journal homepage: www.elsevier.com/locate/developmentalbiology

Hh-induced Smoothened conformational switch is mediated by differential phosphorylation at its C-terminal tail in a dose- and position-dependent manner

Junkai Fan, Yajuan Liu, Jianhang Jia *

Markey Cancer Center, Department of Molecular and Cellular Biochemistry, University of Kentucky, Lexington, KY 40536, USA

ARTICLE INFO

Article history:
Received 25 October 2011
Received in revised form
2 April 2012
Accepted 7 April 2012
Available online 19 April 2012

Keywords:
Smo
PKA
CK1
Phosphorylation
Hh
Signal transduction

ABSTRACT

The activation of Smoothened (Smo) requires phosphorylation at three clusters of Serine residues in *Drosophila* Hedgehog (Hh) signaling. However, the mechanism by which phosphorylation promotes Smo conformational change and subsequently activates Smo in response to Hh gradient remains unclear. Here, we show that the conformational states of Smo are determined by not only the amount but also the position of the negative charges provided by phosphorylation. By using a Smo phospho-specific antibody, we demonstrate that Smo is differentially phosphorylated at three clusters of serine residues in response to levels of Hh activity. Mutating the first cluster, compared to mutating the other clusters, impairs Smo activity more severely, whereas mutating the last cluster prohibits C-terminus dimerization. In addition, phosphorylation of the membrane proximal cluster promotes phosphorylation of the distal cluster. We propose a zipper-lock model in which the gradual phosphorylation at these clusters induces a gradual conformational change in the Smo cytoplasmic tail, which promotes the interaction between Smo and Costal2 (Cos2). Moreover, we show that Hh regulates both PKA and CK1 phosphorylation of Smo. Thus, the differential phosphorylation of Smo mediates the thresholds of Hh activity.

Introduction

The Hedgehog (Hh) morphogen controls several key development processes in a concentration-dependent manner (Ingham and McMahon, 2001; Ingham et al., 2011; Jiang and Hui, 2008; Riddle et al., 1993; Roelink et al., 1995). In *Drosophila*, Hh protein plays a broad role in the development of appendages, such as wings, eyes, and legs. One of the best systems for studying Hh signaling is the wing imaginal disc, in which the posterior (P) compartment cells express and secrete Hh proteins that act upon neighboring anterior (A) compartment cells located adjacent to the A/P boundary to induce the expression of *decapentaplegic* (*dpp*), which encodes a member of the TGFβ/BMP family of secreted proteins (Basler and Struhl, 1994; Tabata and Kornberg, 1994). The Dpp protein then diffuses bidirectionally into both the A and P compartments and functions as a morphogen to control the growth and patterning of cells in the entire wing in a concentration-dependent manner (Campbell and Tomlinson, 1999; Lecuit et al., 1996; Nellen et al., 1996). Hh also specifies cell patterning at the A/P boundary by activating other genes, including *engrailed* (*en*) and *ptc* (Strigini and Cohen, 1997; Vervoort et al., 1999). Low levels of Hh are able to induce the expression of *dpp*, whereas higher levels of Hh are also able to activate *ptc*. The induction of *en* appears to require the highest doses of Hh signaling activities (Strigini and Cohen, 1997). Thus, Hh activity levels can be monitored by expression of different responsive genes. Based on these findings, it is important to understand how cells perceive and transduce signal gradients, and how these gradients induce differential cell fates.

The receptor complex of Hh signaling consists of Patched (Ptc) and Ihog (Zheng et al., 2010). The seven-transmembrane protein Smoothened (Smo) acts as a signal transducer, and its activity is inhibited by Ptc in the absence of Hh (Hooper and Scott, 2005; Jia and Jiang, 2006; Lum and Beachy, 2004). Binding of Hh to Ptc-Ihog relieves Smo from Ptc inhibition, allowing Smo to activate the Cubitus interuptus (Ci)/Gli family of Zn-finger transcription factors, which induces the expression of Hh target genes (Hooper and Scott, 2005; Jia and Jiang, 2006). The presence of Hh promotes the cell surface accumulation and phosphorylation of Smo (Denef et al., 2000) by protein kinase A (PKA), casein kinase 1 (CK1) (Apionishev et al., 2005; Jia et al., 2004; Zhang et al., 2004), casein kinase 2 (CK2) (Jia et al., 2010), and G protein-coupled receptor kinase 2 (GRK2) (Chen et al., 2010) at the C-terminal cytoplasmic tail (C-tail) of Smo. Phosphorylation promotes Smo activation by inducing a conformational change in the protein (Zhao et al., 2007), which most likely promotes the interaction between

* Corresponding author. Fax: +1 859 257 6030.
E-mail address: Jianhang.jia@uky.edu (J. Jia).

0012-1606/$ - see front matter © 2012 Elsevier Inc. All rights reserved.
http://dx.doi.org/10.1016/j.ydbio.2012.04.007

Smo and the Costal2-Fuses (Cos2-Fu) protein complex (Jia et al., 2003; Lum et al., 2003; Ogden et al., 2003). In addition, the levels of Smo activity are closely correlated with the levels of Smo phosphorylation (Jia et al., 2004; Zhao et al., 2007). Among the kinases identified to date, PKA and CK1 play an essential role in activating Smo by phosphorylating Smo at three clusters of Serine residues in its C-tail (Aikin et al., 2008; Zhao et al., 2007). One important question is how phosphorylation of Smo at the three clusters contributes to its activity. It has been shown that these phosphorylation events counteract the autoinhibition imposed by adjacent clusters of arginine residues (Zhao et al., 2007). Phosphorylation at individual clusters neutralizes the adjacent arginine motifs and induces an open conformation, which promotes Smo dimerization (Jiang and Hui, 2008). However, it is unclear how phosphorylation counteracts the positive charges that are exerted by the arginine clusters.

In this study, by using a Smo phospho-specific antibody, we found that Smo is differentially phosphorylated in response to different levels of Hh signaling activity. We also found that in addition to the number of phosphorylated sites, the position of the phosphorylated residues is critical for establishing the stoichiometry of Smo activity. A phospho-deficient mutation at the first cluster reduces Smo activity more severely than mutation at the other clusters. In contrast, a phosphomimetic mutation of the first cluster induces Smo activity to a higher level than a phosphomimetic mutation at the other individual clusters. We further found that phosphorylation at the first cluster promotes the phosphorylation at the second cluster.

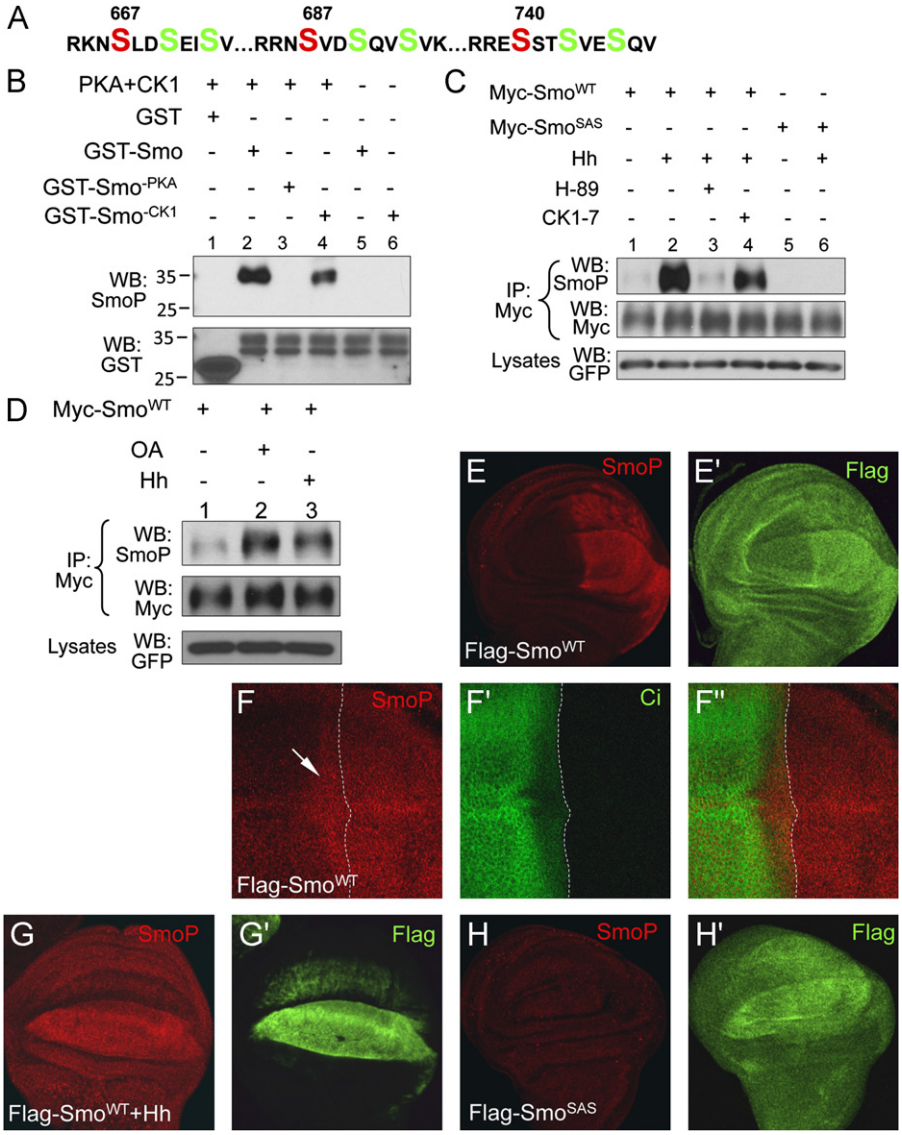

Fig. 1. Characterization of a Smo phospho-specific antibody (SmoP). (A) Smo sequence indicating the three phosphorylation clusters located in the C-tail, with PKA sites marked in red and CK1 sites in green. (B) Smo phosphorylation by PKA and CK1 is detected by the anti-SmoP antibody. An *in vitro* kinase assay is shown here using the purified GST-Smo proteins and the commercial PKA and CK1 kinases. GST is used as a control. (C) S2 cells were transfected with Myc-Smo^{WT} or Myc-Smo^{SAS} and treated with HhN-conditioned medium or control medium, in combination with H-89 and/or CK1–7 inhibitors. To normalize the levels of Smo, 50 μM MG132 and 15 mM NH4Cl was used to block Smo degradation, and samples were normalized for loading. All figures in this study showing the levels of Myc-Smo were normalized by this method. Cell extracts were immunoprecipitated with the anti-Myc antibody and blotted with either anti-Myc to detect Smo phosphorylation, indicated by its mobility shift on the SDS gel, or anti-SmoP, to directly detect Smo phosphorylation. GFP served as a transfection and loading control. (D) S2 cells were transfected with Myc-Smo^{WT} and treated with OA or HhN-conditioned medium followed by immunoprecipitation with the anti-Myc antibody and western blot with anti-Myc or anti-SmoP antibodies. GFP served as a transfection and loading control. Myc-Smo was normalized by the method described above. (E–E′) A wing disc expressing Flag-Smo^{WT} under *MS1096* Gal4 control were immunostained with anti-SmoP and anti-Flag antibodies. (F–F″) A large magnification of a wing disc expressing Flag-Smo under MS1096 Gal4. The arrow indicates SmoP staining in A compartment cells near the A/P boundary. The dash line indicates the A/P boundary that is marked by Ci staining. (G–H′) Wing discs expressing Flag-Smo^{WT} with Hh or Flag-Smo^{SAS} by *MS1096*-Gal4 were stained for SmoP and Flag. All wing imaginal discs shown in this study were oriented with anterior on the left and ventral on the top.

In addition, although CK1 phosphorylation is primed by PKA phosphorylation at adjacent sites, we provide evidence that phosphomimetic mutations at PKA sites do not constitutively promote CK1 phosphorylation, and that CK1 phosphorylation is regulated by Hh. We propose a zipper-lock model in which phosphorylation at the three clusters of serine residues promotes a gradual conformational change to activate Smo.

Results

Generation and characterization of a Smo phospho-specific antibody

Hh signaling induces Smo C-tail phosphorylation at three clusters of serine residues, including three typical PKA sites that are each followed by two CK1 sites (Fig. 1A). Our understanding of

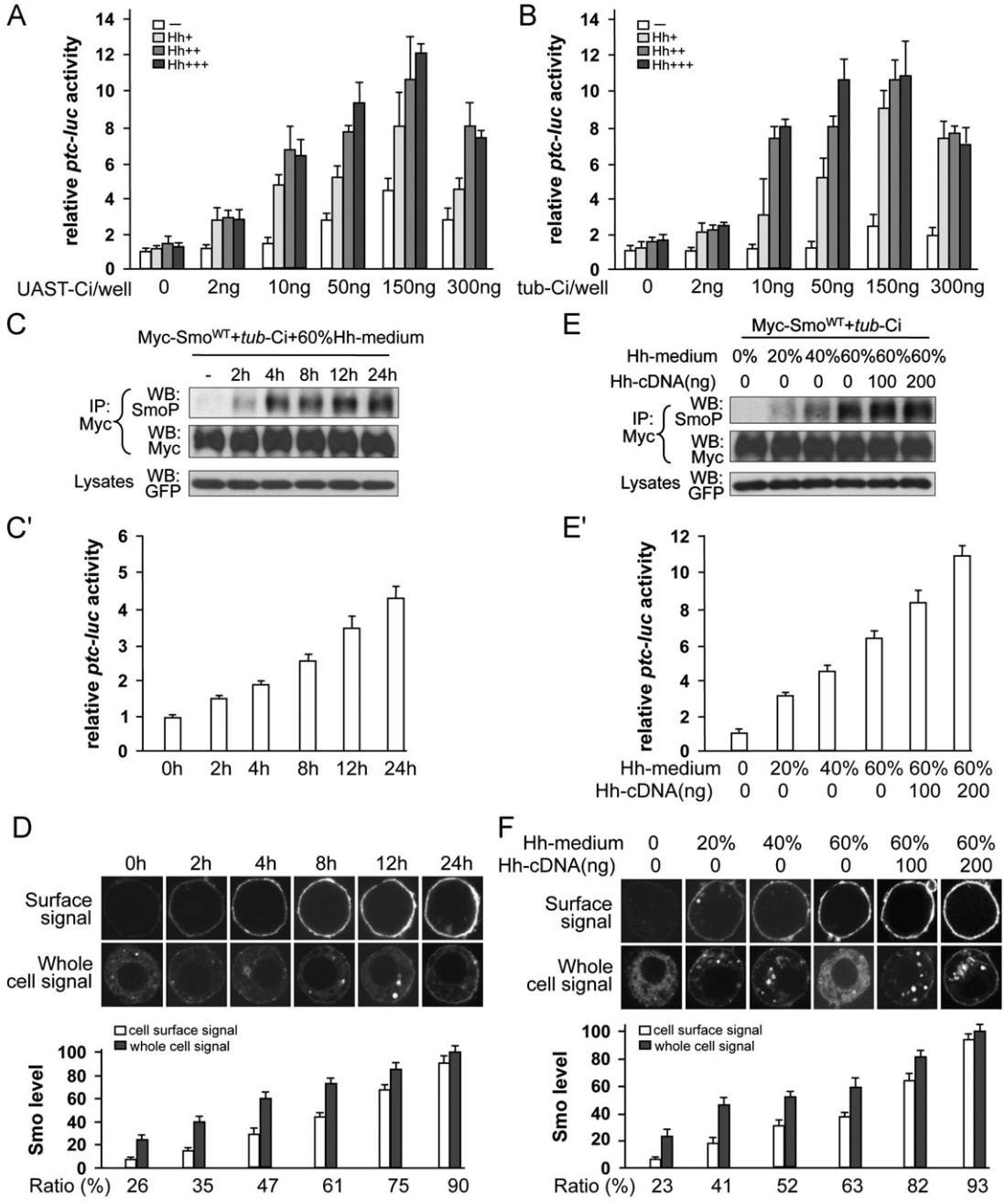

Fig. 2. Gradient of Hh signaling activity induces differential phosphorylation of Smo. (A–B) A *ptc-luc* reporter assay in S2 cells. S2 cells in 6-well plates were co-transfected with 40 ng (Hh+), 80 ng (Hh++), or 160 ng (Hh+++) of UAST-HhN and the indicated amount of either UAST-Ci or *tub*-Ci. The *y*-axis represents normalized *ptc-luc* activity. (C–C') A time course experiment using S2 cells co-transfected with Myc-Smo^{WT} and *tub*-Ci and treated with 60% of Hh-medium in 6-well plates. Cells were then split into two halves, one half for detection of Smo phosphorylation by western blot analysis using the Myc-IP followed by western blot with the anti-Myc or anti-SmoP antibodies, and the second half for the luciferase assay. Myc-Smo was normalized by the method described above. (D) A time course experiment to examine Smo cell surface accumulation by using the same treatments of S2 cells as used for C–C'. Cells were immunostained with the anti-SmoN antibody before membrane permeabilization to visualize cell surface Smo (top panel). Quantification of cell surface and total Smo levels is shown in the bottom panel (mean ± SD; $n \geq 20$). The numbers below the bars indicate the percentage of Smo on the cell surface. The intensity of whole cell signal from 24 h treatment was set as 100. (E–E') S2 cells in 6-well plates were co-transfected with the indicated construct and treated with different amounts of Hh-medium. The cells were then split into two halves, one for detection of Smo phosphorylation, and the second for the luciferase assay. Myc-Smo was normalized by the method described above. (F) A parallel experiment similar to that used in E–E' to examine Smo cell surface accumulation under different conditions. Quantification is shown in the bottom panel (mean ± SD; $n \geq 20$). The numbers below the bars indicate the percentage of Smo on the cell surface. The intensity of whole cell signal from the highest Hh treatment was set as 100.

Smo phosphorylation by PKA and CK1 kinases has been derived mainly from a combination of *in vitro* kinase assays and *in vivo* functional assays of phosphorylation sites mutations. The phosphorylation of individual sites *in vivo* and its regulation by different levels of Hh activity has not been determined. As a first step toward addressing this important issue, we generated an antibody to specifically detect phosphorylation at the 2nd cluster (anti-SmoP). To characterize this antibody, we carried out an *in vitro* kinase assay by using the commercial PKA/CK1 kinases and glutathione *S*-transferase (GST)-Smo fusion proteins. GST-Smo^{-PKA} has an S > A mutation in the PKA site and GST-Smo^{-CK1} has S > A mutations in the two CK1 sites of the 2nd phosphorylation cluster. As shown in Fig. 1B, phosphorylation of GST-Smo by PKA and CK1 was detected by the anti-SmoP antibody (Fig. 1B, lane 2, top panel). Mutation in the PKA site in the 2nd cluster abolished phosphorylation by PKA and CK1, as shown by the loss of signal in the western blot using the anti-SmoP antibody (lane 3, top panel). Mutations in CK1 sites blocked phosphorylation by CK1 but did not affect the phosphorylation of the PKA site (lane 4, top panel). The anti-SmoP antibody did not recognize the unphosphorylated forms of Smo (lanes 5–6, top panel). These results indicate that the phospho-specific SmoP antibody is able to detect both PKA and CK1 phosphorylation within the 2nd cluster.

To determine whether the anti-SmoP antibody was able to detect *in vivo* phosphorylation of Smo, we transfected S2 cells with Myc-tagged full-length wild-type Smo (Myc-Smo^{WT}) or Myc-tagged Smo containing a mutation in the PKA site of the second cluster to alanine (Myc-Smo^{SAS}), and then treated the transfected cells with HhN-conditioned medium with or without the PKA inhibitor H-89 or CK1 inhibitor CK1-7 as previously described (Jia et al., 2004). Hh consistently induced Smo phosphorylation, which was readily detected by the anti-SmoP antibody (Fig. 1C, lane 2, top panel). H-89 severely reduced the SmoP signals, whereas CK1-7 had only a slight effect (Fig. 1C, lanes 3–4). Myc-Smo^{SAS} was not phosphorylated in either the presence or absence of Hh (Fig. 1C, lanes 5–6). Treatment with the phosphatase inhibitor okadaic acid (OA) enhanced the SmoP signal (Fig. 1D, lane 2, top panel). These data indicate that the anti-SmoP antibody is able to detect Smo phosphorylation at PKA and CK1 sites located within the second cluster in cultured S2 cells.

We also performed immunostaining with the anti-SmoP and anti-Flag antibodies in wing imaginal discs expressing Flag-tagged wild-type Smo (Flag-Smo^{WT}). We found that there was a strong signal for the anti-SmoP antibody in P compartment cells where Hh was present, but a very low signal in A compartment cells that were located away from the A/P boundary where Hh was not present (Fig. 1E). In addition, Hh induced a SmoP staining gradient in A compartment cells near the A/P boundary (arrow in Fig. 1F). Moreover, the coexpression of Hh induced a strong anti-SmoP antibody signal in A compartment cells (Fig. 1G). In contrast, there was no signal detected by the anti-SmoP antibody when Smo^{SAS} was expressed (Fig. 1H). These data indicate that the anti-SmoP antibody is able to detect Hh-induced phosphorylation of Smo in wing discs.

The Hh activity gradient induces differential phosphorylation and cell surface accumulation of Smo

It has been postulated that different levels of Hh signaling activity can induce different levels of Smo phosphorylation (Jia et al., 2004; Zhao et al., 2007). However, a direct link between the Hh signaling activity and the phosphorylation of Smo has not been shown. To address this issue, we first established a *ptc-luciferase* (*ptc-luc*) reporter assay to monitor the activity of Hh signaling. As shown in Fig. 2A, the increasing expression *UAST-HA-Ci* by *ub*-Gal4 induced increasingly higher level of *ptc-luc* reporter activity (Fig. 2A, compare the first column in groups 1–5). The coexpression of increasing amounts of *UAST-HhN* induced *ptc-luc* reporter activity in a dose-dependent manner, suggesting a response of S2 cells to Hh activity in the presence of transfected Ci. Therefore, we next assessed whether the expression of Ci at the endogenous level would work better under this situation in order to examine the responsiveness to Hh. We generated a *tub-Ci* construct where the *UAS* binding sites in *pUAST* were replaced by the *tubulinα* promoter to drive *ci* expression at a level close to that of the endogenous gene expression (Basler and Struhl, 1994; Jia et al., 2010). We found that the expression of Ci by the *tubulinα* promoter was able to mediate differential Hh activity, as assessed by *ptc-luc* reporter activity (Fig. 2B). We normalized *tub-Ci* conditions in this assay and chose the best responsive condition as a standard for subsequent experiments (Fig. 2B, group 4).

We then assessed the correlation of Hh signaling activity to the levels of Smo phosphorylation by using the anti-SmoP antibody. S2 cells were co-transfected with Myc-Smo^{WT} and *tub*-Ci followed by treatment with HhN-conditioned medium. As shown in Fig. 2C, after collecting the cells at different time points, we found that Hh induced a higher level of Smo phosphorylation when the cells were exposed to Hh for a longer period of time. The Hh activity was monitored by *ptc-luc* reporter activity (Fig. 2C′). The assessment of cell surface accumulation has been successfully used to examine Smo activation in our previous studies, and therefore we performed the same set of experiments to monitor the cell surface accumulation of Smo. We found that Hh induced the cell surface accumulation of Smo in a time-dependent manner (Fig. 2D), suggesting a close correlation between phosphorylation and cell surface accumulation. In a parallel experiment, we examined Smo phosphorylation and cell surface accumulation when the cells were treated with different amounts of Hh. As shown in Fig. 2E, different levels of Hh activity induced different levels of Smo phosphorylation, as indicated by the strength of the anti-SmoP antibody signal (Fig. 2E, top panel). The gradient Hh activity was monitored by *ptc-luc* reporter activity (Fig. 2E′). We further found that Hh induced the cell surface accumulation of Smo in a dose-dependent manner (Fig. 2F). Taken together, by combining the luciferase and cell surface staining assays with a phosphorylation assay using an anti-SmoP antibody, we were able to precisely correlate the levels of phosphorylation and cell surface accumulation of Smo to the levels of Hh signaling activity.

Substitution of the phosphorylation clusters does not change the activity of Smo

To explore the contribution of phosphorylation at the three clusters to Smo activity, we substituted the 1st cluster and 3rd cluster with the 2nd cluster to create Smo^{222} (Fig. 3A). We then generated transgenes using the PhiC31 integration system to integrate Myc-tagged Smo^{222} (Myc-Smo^{222}) or Smo^{222} in combination with the *tubulinα* promoter (tub-Smo^{222}) into the 75B1 attP locus in the fly genome in order to examine the precise activity of Smo^{222} (Bischof et al., 2007; Jia et al., 2010). The expression of *ptc* and *en* were blocked in *smo* mutant cells of wing imaginal discs (arrows in Fig. 3B and C). We found that the expression of Myc-Smo^{222} under control of *MS1096* Gal4 or Smo^{222} under the *tubulinα* promoter fully rescued *ptc* and *en* expression in *smo* mutant cells (arrows in Fig. 3D–G), similar to the rescue of Smo^{WT} driven by the *tubulinα* promoter or by *MS1096* Gal4 (Jia et al., 2010, 2003). In addition, overexpression of Myc-Smo^{222} induced a comparable level of ectopic *dpp-lacZ* expression (Fig. 3I) similar to that of Myc-Smo^{WT} (Fig. 3H). The anti-SmoP antibody was not able to detect the phosphorylation of endogenous Smo in wing discs. However, there was a clear increase in affinity of the anti-SmoP antibody for Smo^{222},

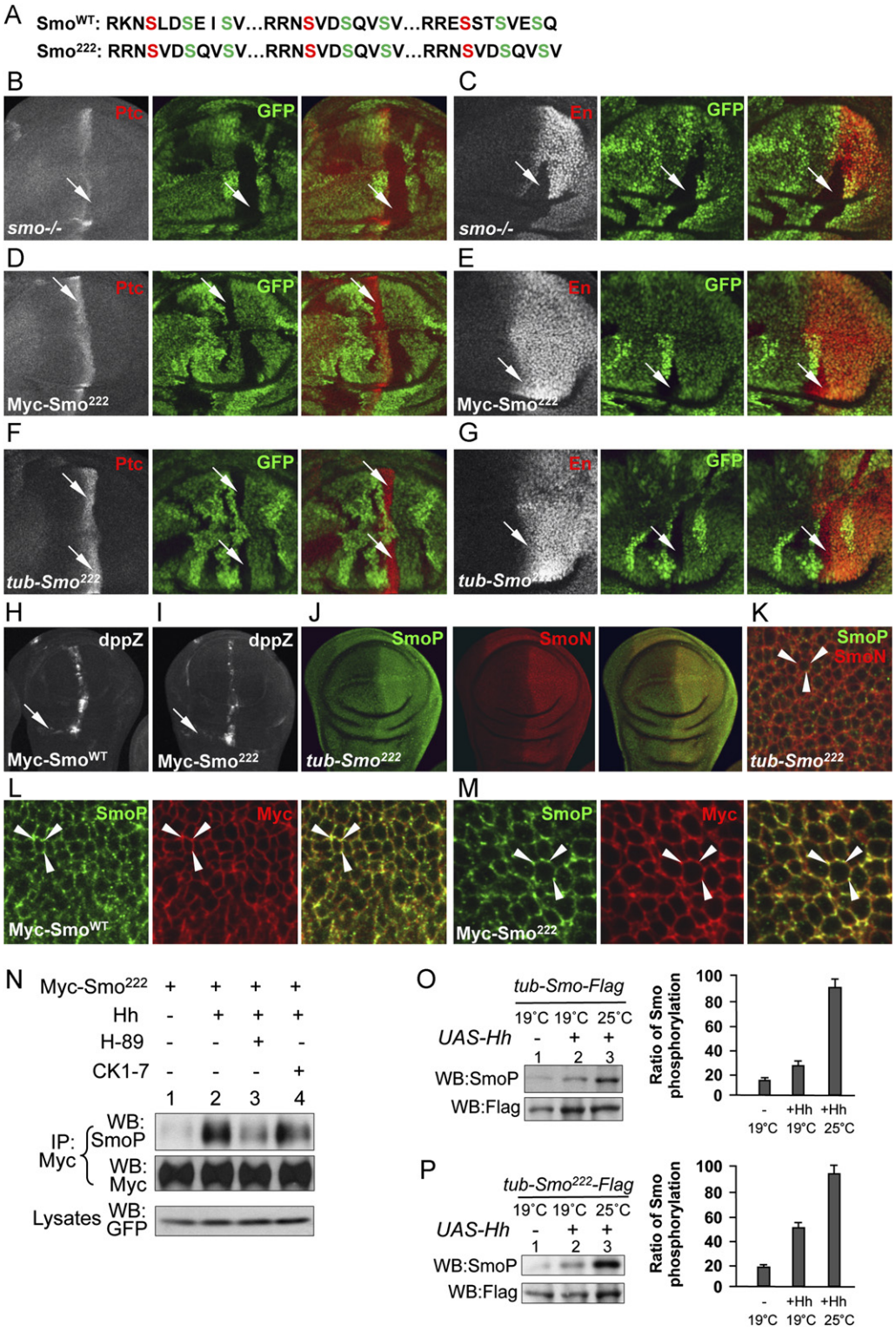

Fig. 3. Changing the sequence of the phosphorylation clusters has no effect on Smo activity and responsiveness to Hh. (A) Sequence alignment of Smo^{WT} and Smo^{222} in which the 1st and 3rd clusters were substituted with the 2nd cluster. (B and C) Wing discs carrying *smo* mutant clones immunostained for Ptc (red), En (red), or GFP (green). The *smo* mutant clones were recognized by the lack of GFP expression and the A/P boundaries were determined by Ci staining (not shown). (D–G) Wing discs containing *smo* mutant clones and expressing either Myc-Smo^{222} by *MS1096* Gal4 or Smo^{222} by the *tubulinα* promoter were immunostained to show Ptc, En, and GFP. The arrows indicate the rescued *ptc* or *en* expression by expressing Smo^{222} in *smo* cells. (H and I) Wing discs expressing Myc-Smo^{WT} or Myc-Smo^{222} by *MS1096* Gal4 were stained for *dpp-lacZ* expression. The arrows indicate the comparable *dpp-lacZ* expression when either forms of Smo are expressed. (J) A wing discs expressing Smo^{222} by the *tubulinα* promoter is stained for SmoP and SmoN. (K) A large magnification image of the P compartment in the wing disc from Figure J. The arrowheads indicate the co-localization of SmoP and SmoN on the cell membrane. (L and M) Large magnification images of the cells in P compartment of the wing discs expressing either Myc-Smo^{WT} or Myc-Smo^{222}. The arrowheads indicate the co-localization of Myc and SmoP signals. (N) S2 cells were transfected with Myc-Smo^{222} and treated with Hh-medium in combination with H-89 or CK1–7. Cell lysates were subjected to immunoprecipitation with anti-Myc followed by a western blot with anti-Myc or anti-SmoP antibodies. GFP served as a transfection and loading control. Myc-Smo was normalized by the method described above. (O and P) Wing discs expressing Smo^{WT} or Smo^{222} by the *tubulinα* promoter, or co-expressing Smo^{WT} or Smo^{222} by the *tubulinα* promoter along with *UAS-Hh* by *MS1096* Gal4 were collected from flies cultured at either 25 °C or 19 °C, and then subjected to direct western blot with the anti-SmoP antibody to detect the phosphorylated forms of Smo^{WT} or Smo^{222}, or with anti-Flag antibody to detect the total Smo. The ratio of phosphorylated Smo to total Smo is shown in the right panel (each data set was from three repeats).

as shown by the signal of the anti-SmoP antibody in P compartment cells (Fig. 3J) as well as A compartment cells near the A/P boundary (not shown). These results indicated that Hh-induced *tub-Smo*^{222} phosphorylation can be detected *in vivo*. Furthermore, the anti-SmoP signal was mostly present at the plasma membrane of P compartment cells, and the anti-SmoP signal co-localized very well with the signal from the anti-SmoN antibody, which recognizes the N-terminal extracellular domain of Smo (arrowheads in Fig. 3K). Moreover, the anti-SmoP signal co-localized with the anti-Myc signal in P compartment cells expressing either Myc-Smo^{WT} or Myc-Smo^{222} under control of *MS1096* Gal4 (arrowheads in Fig. 3L and M). These data indicate that Smo^{222} functions similarly to Smo^{WT}.

We next examined the phosphorylation of Smo^{222} in both cultured S2 cells and wing discs by western blot. As shown in Fig. 3N, Hh-induced Smo^{222} phosphorylation was detectable by the anti-SmoP antibody and was diminished by treatment with H-89 (Fig. 3N, lane 3, top panel), but attenuated by treatment with CK1-7 (Fig. 3N, lane 4, top panel). To examine whether different levels of Hh activity induce different levels of Smo phosphorylation in wing discs, we expressed either *tub-Smo*^{WT} or *tub-Smo*^{222} together with *UAS-Hh* driven by *MS1096* Gal4 in wing discs at different temperatures. We found that a higher level of Hh expression at a higher temperature induced a higher phosphorylation level of both Smo^{WT} and Smo^{222} compared to lower Hh expression at a lower temperature (Fig. 3O and P). Smo phosphorylation in the absence of *UAS-Hh* indicated that Smo phosphorylation occurred in P compartment cells where endogenous Hh was expressed (lane 1 in Fig. 3O and P, top panel). The use of the *tubulinα* promoter ensured equal levels of Smo expression (Fig. 3O and P, lower panel). These data provide another direct detection of *in vivo* Smo phosphorylation, which is regulated by the Hh threshold. Similarly, the substitution of the 1st cluster with the 2nd cluster (Smo^{223}) fully rescued the *smo* mutant, had comparable activity as Smo^{222} in the ability to induce ectopic *dpp-lacZ* expression, and exhibited a similar phosphorylation pattern to that of Smo^{222} (data not shown). Taken together, our results indicate that substitution among the three clusters did not changed Smo activity or affect its responsiveness to Hh stimulation.

Phosphorylation at 3 clusters does not equally contribute to Smo activity

To investigate how phosphorylation regulates Smo activity, we constructed a series of Smo mutants with different combinations of PKA and CK1 site mutations (Figs. 4A, 5A). To ensure that Smo was expressed at the same level without positional effects, we generated all of the transgenes at the 75B1 attP locus. Expression of Smo^{WT} induced a low level of ectopic *dpp-lacZ* expression (Fig. 4B) (Jia et al., 2003), whereas expression of Smo^{DDD} (previously named Smo^{SD123}) induced full *dpp-lacZ* expression in A compartment cells (Fig. 4C) (Jia et al., 2004). Phosphomimetic mutations of each cluster (Smo^{DSS}, Smo^{SDS}, Smo^{SSD}; Fig. 4A) elevated Smo activity, as evidenced by the higher level of ectopic *dpp-lacZ* expression (Fig. 4D–F). A careful comparison indicated that Smo^{DSS} had a higher level of ectopic *dpp-lacZ* expression compared to either Smo^{SDS} or Smo^{SSD} (Fig. 4D compared to Fig. 4E and F). We further generated combinations of two cluster phosphomimetic mutations. Consistent with our previous findings, Smo^{DDS} (previously named Smo^{SD12}) induced a further increase of *dpp-lacZ* expression (Fig. 4G) (Jia et al., 2004). Smo^{DSD} induced ectopic *dpp-lacZ* expression at a level that was lower than that induced by Smo^{DDS} (Fig. 4H). Interestingly, Smo^{SDD} was unable to induce a further increase in *dpp-lacZ* expression (compared to Smo^{DSS}, Smo^{SDS}, or Smo^{SSD}), even though two of the three clusters were mutated to aspartate (Fig. 4I). These results suggested that sequential phosphorylation at the first two clusters is critical for Smo activation and that the position of phosphorylation plays a role in activating Smo. We then generated Smo^{ADD}, Smo^{DAD}, and Smo^{DDA} mutations (Fig. 4A). Surprisingly, the activity of Smo^{DDA} was dramatically impaired by an S > A mutation at the 3rd cluster (Fig. 4L compared to 4G). Smo^{ADD}, Smo^{DAD}, and Smo^{DDA} induced a low level of *dpp-lacZ* expression, which was comparable to Smo^{WT} (Fig. 4J–L). In addition, the expression of Smo^{ADD}, Smo^{DAD}, and Smo^{DDA} at a higher temperature (30 °C) did not elevate their activity (Fig. 4A), indicating that S > A mutations severely interfered with the activity of Smo phosphomimetic mutants. However, Smo^{DDA} restored *dpp-lacZ* expression and partially rescued *ptc* expression, but did not rescue *en* expression in *smo* mutant cells near the A/P boundary, suggesting that it could transduce low, but not high, levels of Hh activity (Fig. 4A, data not shown). The changes in Smo activity induced by these mutations were confirmed by the *ptc-luc* reporter assay (Fig. 4R).

We next assessed the activation of these mutants by measuring Smo cell surface accumulation. We found that Smo^{ADD}, Smo^{DAD}, and Smo^{DDA} exhibited a very low accumulation at the cell surface (Fig. 4S, columns 9–11), which provided an explanation of the inactivity in the wing discs. The cell surface accumulation of the other Smo variants was consistent with their individual activity in the imaginal discs (Fig. 4S).

Hh induces Smo dimerization at its C-terminal tail (Zhao et al., 2007). Our finding that the *in vivo* activity and the cell surface accumulation of Smo^{DDA} were severely impaired by the S > A mutation at the 3rd cluster prompted us to examine whether this mutation blocks C-terminal dimerization. Therefore, we used the fluorescence resonance energy transfer (FRET) assay to test C-terminal CFP/YFP dimerization. Consistent with the findings of Zhao and colleagues (Zhao et al., 2007), Smo^{DDD} had a very high FRET signal compared to Smo^{WT} (Fig. 4T, columns 1–2). We further found that Smo^{DDA} had much lower FRET signal and was much less responsiveness to Hh stimulation compared to Smo^{DDS} (Fig. 4T), suggesting that the phospho-deficient mutation at the 3rd cluster blocks the dimerization of Smo at the C-tail. Other Smo mutations exhibited different levels of FRET signal, which was consistent with their *in vivo* activity (Fig. 4T and S1).

We next examined the dominant-negative activity of Smo mutants that possessed two clusters of S > A mutations (Fig. 5A). We found that Smo^{AAD}, Smo^{AAS}, and Smo^{SAA} have dominant negative activity, as indicated by their ability to block *ptc-lacZ* and *en* expression in A compartment cells near the A/P boundary (Fig. 5B and C, H and I, L and M). Consistent with this finding, *tub-Smo*^{AAS} and *tub-Smo*^{SAA} did not rescue *ptc* and *en* expression in *smo* null mutant cells (Fig. 5P and S). We also found that Smo^{AAS} had stronger dominant-negative activity than Smo^{SAA}, since Smo^{AAS} blocked *en* expression in the wing disc more severely than Smo^{SAA} (Fig. 5I) and caused further fusion between vein 3 and vein 4 (Fig. S2C), which is indicative of loss of Hh signaling in the wings (Liu et al., 2007). Interestingly, we found that overexpression of Myc-Smo^{ADA}, Smo^{DAA}, and Smo^{ASA} did not cause any dominant-negative effects in wing discs, which was likely due to the split of the mutation sites or the ability of the S > D mutations to counteract the S > A mutations (Figs. 5D–G, and J and K). We further evaluated our findings by using the *ptc-luc* reporter and FRET assays. As shown in Fig. 5T, expression of Smo^{ADA} Smo^{DAA}, and Smo^{ASA} did not induce *ptc-luc* activity. Expression of Smo^{AAD}, Smo^{AAS}, or Smo^{SAA} exhibited lower *ptc-luc* activity compared to control, indicating their dominant-negative activity in this assay (Fig. 5T, columns 3, 6, 8, and 9). In addition, these mutations were barely responsive to Hh in terms of the levels of FRET signal (Fig. 5U). Consistent with our previous findings, mutation in one PKA site (Smo^{ASS}, Smo^{SAS}, and Smo^{SSA}),

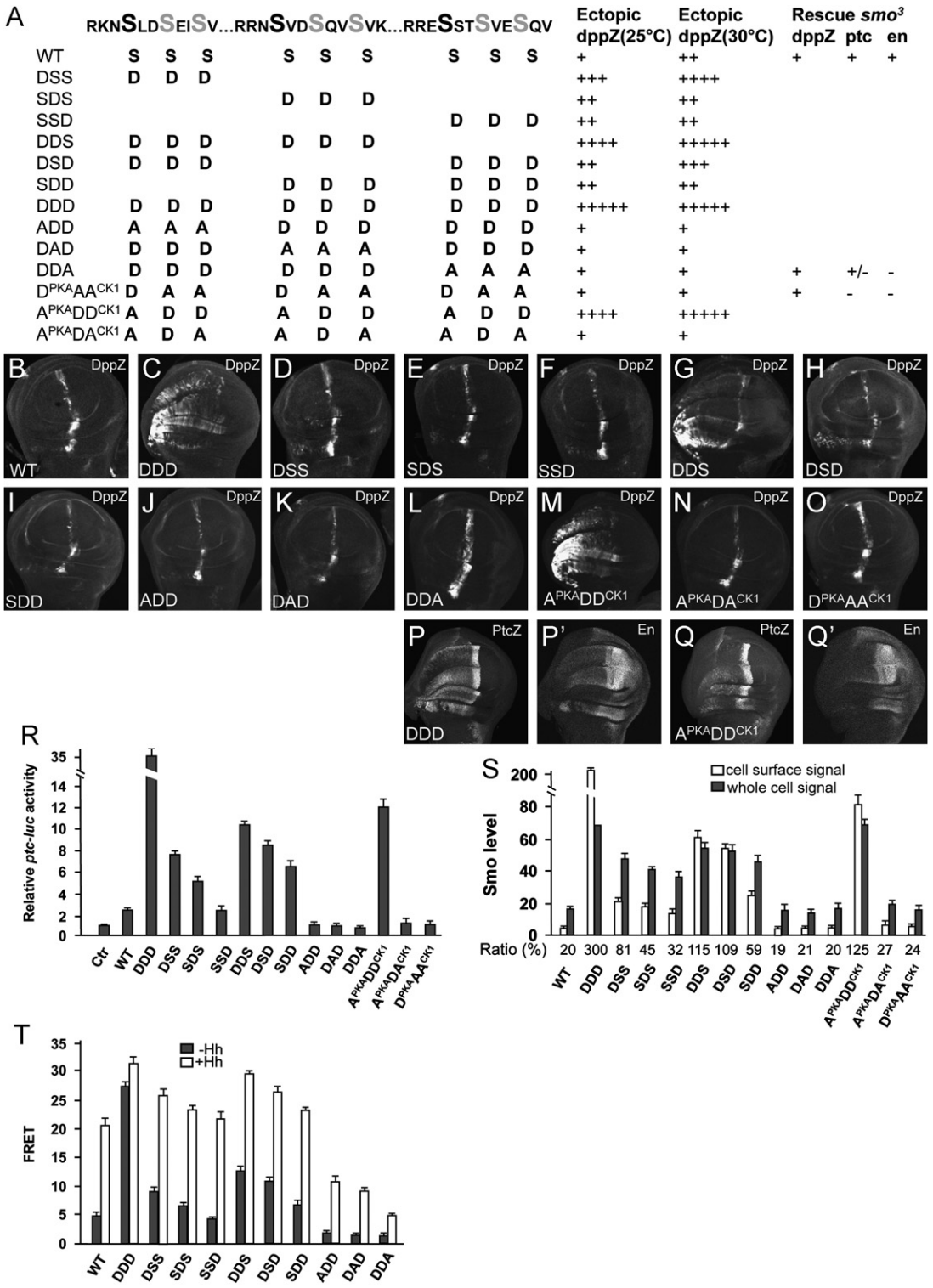

Fig. 4. Intra-molecular mutations contribute differently to Smo activity. (A) A schematic drawing of Smo variants and their *in vivo* activity. In the sequence, enlarged black Ser residues are the PKA sites and enlarged grey Ser residues are CK1 sites. Individual constructs were assayed for Hh signaling activity by overexpression under the *MS1096* Gal4 driver. Ectopic activity was scored by activated *dpp-lacZ* expression. Rescue experiments were carried out to examine whether expressing the indicated constructs by *MS1096*-Gal4 can restore Hh target gene expression in *smo* mutant cells. (B–O) Examples of the ability of each individual construct to induce ectopic *dpp-lacZ* expression in wing discs, when driven by *MS1096* Gal4. Of note, the activity of Smo^{DDA} is dramatically reduced (L) compared to Smo^{DDS} (G), and the activity of $SmoA^{PKA}DD^{CK1}$ is comparable to Smo^{DDD} by inducing similar ectopic *dpp-lacZ* expression (compare M with C). (P–Q′) Wing discs expressing Smo^{DDD} or $SmoA^{PKA}DD^{CK1}$ were stained for Ptc-lacZ (P and Q) and En (P′ and Q′). (R) The activity of each individual construct was assayed by the *ptc-luc* reporter in S2 cells using the method described above. (S) The cell surface accumulation of each individual construct was measured with anti-SmoN antibody staining by using the method described above. Please note that the cell surface accumulation of Smo^{DDA} is dramatically reduced compared to Smo^{DDS}. (T) FRET efficiency from the indicated WT or mutant Smo with CFP or YFP tagged to their C-termini. Smo^{DDA}, Smo^{DAD}, and Smo^{ADD} have significantly reduced FRET values, and are much less responsive to Hh.

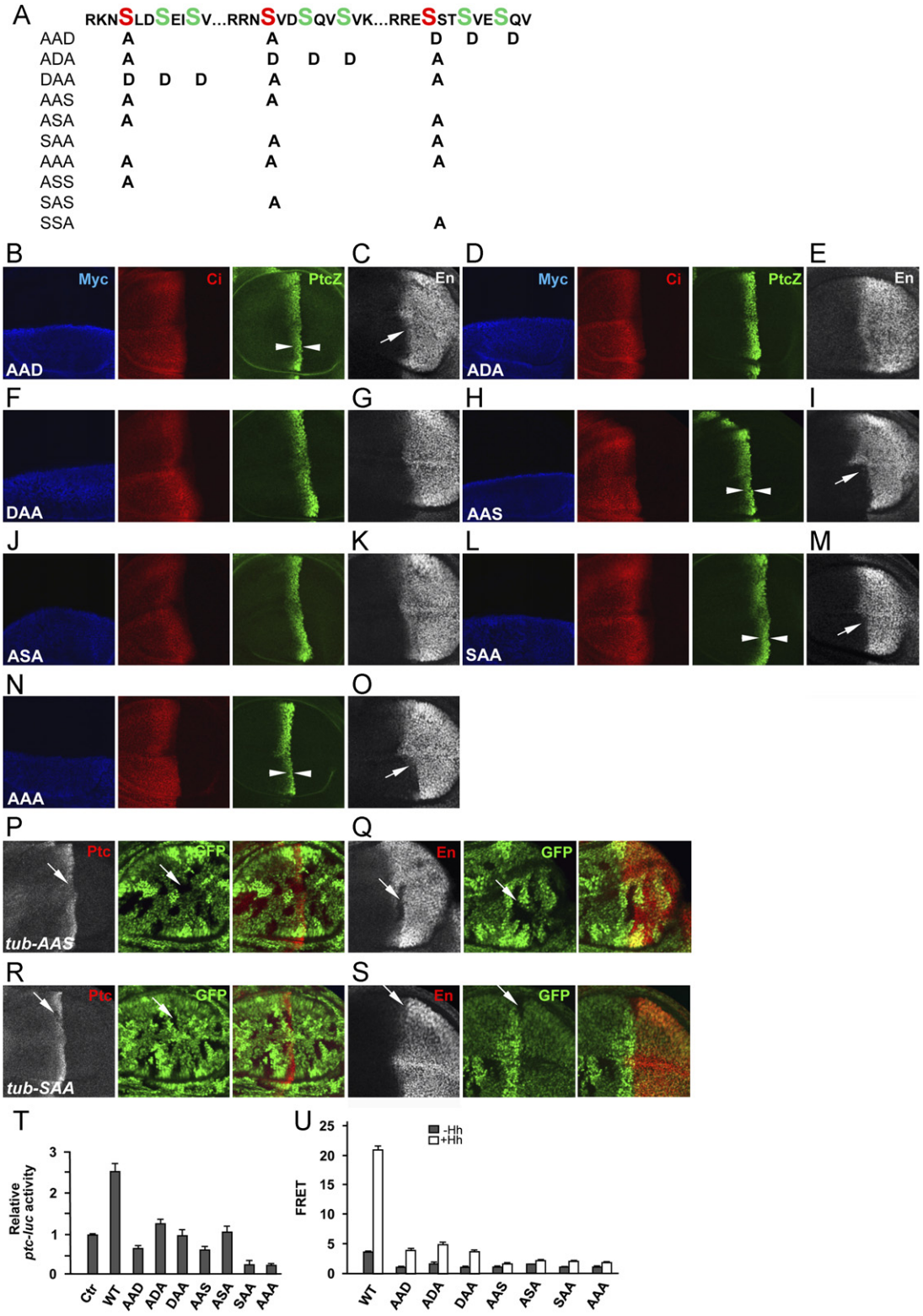

Fig. 5. Dominant-negative activity of Smo with phospho-deficient mutations at different combination of clusters. (A) A schematic drawing of Smo mutants tested in this figure. (B–O) Examples of dominant-negative activity of the indicated Smo constructs when driven by *ap*-Gal4 in wing discs. Arrowheads in B, H, L, and N indicate the constrained *ptc-lacZ* expression in A compartment cells near the A/P boundary. Arrows in C, I, M, and O indicate the attenuated/blockade of *en* expression in A compartment cells near the A/P boundary. The impaired *ptc-pacZ* and *en* expression suggest the dominant-negative activity of each individual Smo construct. (P–S) Wing discs containing *smo* mutant clones and expressing Smo^{AAS} or Smo^{SAA} from the *tubulinα* promoter were immunostained to show Ptc, En, and GFP. The *smo* mutant clones are recognized by the lack of GFP expression. The arrows indicate that Smo^{AAS} and Smo^{SAA} do not rescue *ptc* or *en* expression in cells lacking endogenous *smo*. (T) The *ptc-luc* reporter activity of the indicated Smo constructs that were expressed in S2 cells. (U) FRET efficiency from S2 cells transfected with the indicated Smo constructs and treated with Hh-medium or control medium. Mutations at any of the two clusters interfere with their responsiveness to Hh.

which blocks the phosphorylation of the corresponding cluster, did not change Smo activity, since the expression of these mutants by the *tubulinα* promoter fully rescued *smo* null phenotypes and the overexpression of Myc-tagged mutants caused a similar low level induction of ectopic *dpp-lacZ* expression (data not shown). In contrast, mutations in all three PKA sites (Smo^{AAA}, previously named $Smo^{-PKA123}$) caused Smo to have complete dominant-negative activity, since it extensively blocked *ptc-lacZ* and *en* expression (Fig. 5N and O), severely reduced *ptc-luc* activity (Fig. 5T, column 9), and had an extremely low FRET signal (Fig. 5U, column 8). Taken together, our date suggest a model where phosphorylation promotes Smo activation in a position-dependent manner.

Phosphorylation of membrane proximal cluster promotes phosphorylation of distal cluster

In this study, we found that the adjacent phosphorylation of the first two clusters is critical for Smo activation (Fig. 4). Therefore, we contemplated whether phosphorylation at the 1st cluster facilitated phosphorylation at the other clusters. To assess this possibility, we transfected S2 cells with the Smo construct, treated the cells with HhN-conditioned medium, and then examined Smo phosphorylation status using the anti-SmoP antibody. Hh induced Smo phosphorylation was detected by the signal from the anti-SmoP antibody (Fig. 6A, lane 1, top panel). Mutation of

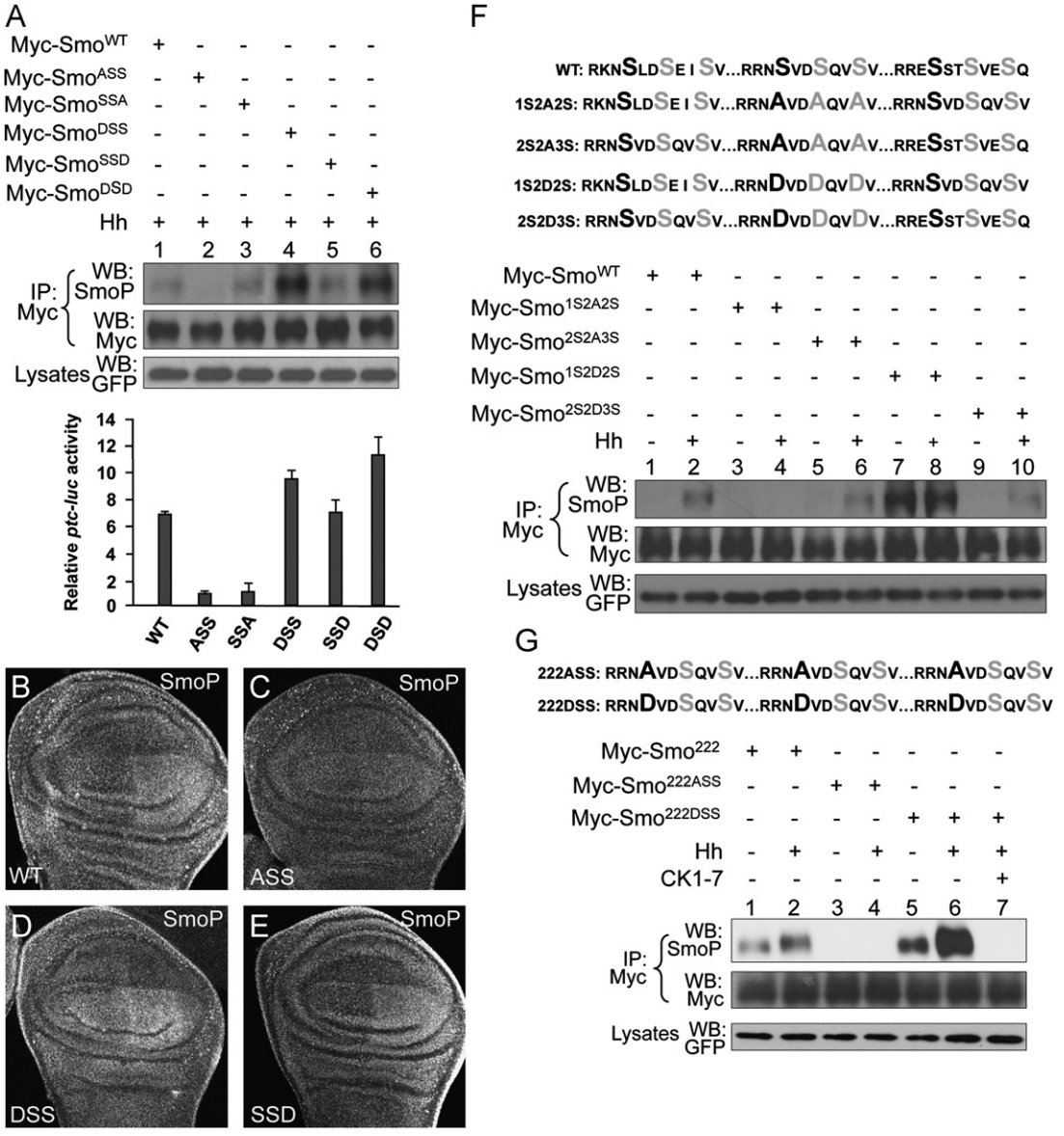

Fig. 6. Phosphorylation at one cluster promotes the phosphorylation at the nearby distal cluster. (A) S2 cells were transfected with the indicated Smo constructs and treated with Hh-medium. Cell extracts were immunoprecipitated with anti-Myc antibody followed by western blot with either anti-SmoP or anti-Myc antibodies. GFP served as a transfection and loading control. Myc-Smo was normalized by the method described above. The bottom panel shows that the same set of Smo constructs were also subjected to luciferase assay in S2 cells with co-transfection of *tub-Ci* and the treatment of Hh-medium. The luciferase value of Smo^{ASS} was set as 1. (B–E) Wing discs expressing the indicated Smo constructs by *MS1096* Gal4 were stained for SmoP. (F) S2 cells were transfected with the indicated Smo constructs and treated with HhN-conditioned medium or control medium. Immunoprecipitation was carried out with the anti-Myc antibody. To detect phosphorylation at a specific position, the anti-SmoP antibody was used to detect phosphorylation of the 2nd cluster sequence. GFP served as a transfection and loading control. Myc-Smo was normalized by the method described above. (G) S2 cells transfected with Myc-Smo^{222DSS} or Myc-Smo^{222ASS} were treated with Hh-medium or control medium. Cell extracts were immunoprecipitated and a western blot was performed with the indicated antibodies. GFP served as a transfection and loading control. Myc-Smo was normalized by the method described above.

the PKA site in the 1st cluster (Myc-Smo^{ASS}) attenuated the phosphorylation at the 2nd cluster, as indicated by the reduction of anti-SmoP signal (lane 2, top panel). Phospho-deficient mutation at the 3rd cluster did not influence phosphorylation at the 2nd cluster (lane 3, top panel). In contrast, a phosphomimetic mutation in the 1st cluster promoted phosphorylation at the 2nd cluster (lane 4 and 6, top panel). Moreover, a phosphomimetic mutation at the 3rd cluster did not promote phosphorylation at the 2nd cluster (lane 5, top panel). The phosphorylation of Smo variants was consistent with their activity in luciferase assays (Fig. 6A, bottom panel).

We further examined whether Smo phosphorylation at the second cluster of PKA/CK1 sites is affected by phosphorylation at other clusters in wing discs. As shown in Fig. 6B, Myc-Smo^{WT} was phosphorylated in P compartment cells as well as A compartment cells near the A/P boundary, a similar pattern to that of Flag-Smo (Fig. 1E) but a much weaker anti-SmoP staining due to a lower level expression of the protein at the VK5 locus (Venken et al., 2006). Phospho-deficient mutation at the first PKA/CK1 cluster (Myc-Smo^{ASS}) severely decreased phosphorylation at the second PKA/CK1 cluster (Fig. 6C), whereas phosphomimetic mutation at the first cluster (Myc-Smo^{DSS}) increased the phosphorylation at the second cluster (Fig. 6D). In contrast, phosphomimetic mutation at the third cluster (Myc-Smo^{SSD}) had no effect on the phosphorylation of the second cluster (Fig. 6E). A comparable level of Smo expression was ensured by expression Smo at a specific genomic locus and monitored by staining with the anti-Myc antibody (not shown). These data consistently demonstrate that phosphorylation at the first PKA/CK1 cluster promotes phosphorylation at the second cluster.

To further demonstrate that phosphorylation at one cluster can promote phosphorylation at the distal cluster, we used the anti-SmoP antibody to assess the phosphorylation of Smo mutations. Smo^{1S2A2S} and Smo^{1S2D2S} were created by mutating the 2nd cluster PKA and CK1 sites to either alanine or aspartate and substituting the 3rd cluster with the 2nd cluster (Fig. 6F, sequence alignment). Similarly, Smo^{2S2A3S} and Smo^{2S2D3S} had the 1st cluster substituted with the 2nd cluster and the 2nd cluster PKA and CK1 sites mutated to either alanine or aspartate (Fig. 6F, sequence alignment). We found that deficient phosphorylation at the position of the 2nd cluster (Smo^{1S2A2S}) prevented phosphorylation at the position of the 3rd cluster (Fig. 6F, lanes 3 and 4, top panel), whereas mimicking phosphorylation at the position of the 2nd cluster (Smo^{1S2D2S}) promoted phosphorylation at the position of the 3rd cluster (lane 7, top panel). However, phosphorylation at the position of the 2nd cluster (Smo^{2S2D3S}) did not promote phosphorylation at the position of the 1st cluster (lane 9 compared to lane 3, top panel) and did not affect Hh-induced phosphorylation at the 1st cluster (lane 10 compared to lane 4, top panel). Taken together, these data suggest that phosphorylation at proximal clusters promotes phosphorylation of the distal cluster, and that phosphorylation at a proximal cluster is not influenced by phosphorylation at the distal cluster.

Both PKA and CK1 phosphorylation are regulated by Hh

To examine the contribution of PKA or CK1 phosphorylation to Smo activity, we constructed Myc-SmoA^{PKA}DD^{CK1}, in which the PKA sites were mutated to alanine and CK1 sites were mutated to aspartate in the three clusters (Fig. 4A). SmoA^{PKA}DD^{CK1} and Smo^{DDD} induced comparable levels of ectopic *dpp-lacZ* expression (Fig. 4M, compared to C), which was most likely due to the higher level of cell surface accumulation (Fig. 4S) and suggests that CK1 phosphorylation plays a potent role in Smo activation. We further found that a phosphomimetic mutation at one PKA or CK1 site (SmoA^{PKA}DA^{CK1} and SmoD^{PKA}AA^{CK1}, Fig. 4A) did not affect the activity of Smo (Fig. 4N–O, compared to Smo^{WT}, 4B). These results suggest that phosphorylation leads to Smo activation in a dose-dependent manner.

We next determined if SmoA^{PKA}DD^{CK1} and Smo^{DDD} had equal activity. We found that SmoA^{PKA}DD^{CK1} induced less *ptc-lacZ* and *en* expression in A compartment cells of the wing disc (Fig. 4Q and Q′, compared to Fig. 4P and P′), suggesting that PKA phosphorylation of Smo contributes to Smo activation in addition to its priming role. Consistently, SmoD^{PKA}AA^{CK1} transduced low levels Hh signaling activity by restoring *dpp-lacZ* expression, but not high levels Hh signaling activity because it did not rescue *ptc* and *en* expression in *smo* mutant cells near the A/P boundary (Fig. 4A, data not shown).

PKA phosphorylation primes CK1 phosphorylation at adjacent sites in the phosphorylation clusters. However, it is not known whether PKA phosphorylation constitutively promotes CK1 phosphorylation or whether CK1 phosphorylation is regulated by Hh. To address these questions, we carried out experiments with S2 cells to examine Smo phosphorylation at the three clusters of CK1 sites. We generated Smo^{222ASS} and Smo^{222DSS} in which PKA sites were mutated to either alanine to block PKA phosphorylation or aspartate to mimic PKA phosphorylation, respectively, in the background of Smo^{222}. This approach allowed for the detection of Smo phosphorylation at the positions of three clusters that had higher affinity for the anti-SmoP antibody (Fig. 6G, sequence alignment). Consistently, we found that Hh induced phosphorylation at clusters of PKA and CK1 sites (Fig. 6G, lanes 1–2, top panel), since the anti-SmoP antibody was able to detect both PKA and CK1 phosphorylation (Fig. 1). We further found that a phosphomimetic mutation at the PKA sites (Smo^{222DSS}) induced lightly higher CK1 phosphorylation at adjacent sites when Hh was absent (Fig. 6G, lane 5 compared to lane 1, top panel), but induced CK1 hyperphosphorylation when Hh was present (lane 6, top panel), suggesting that CK1 phosphorylation is regulated by Hh. Smo^{222ASS} was not phosphorylated either in the presence or absence of Hh (Fig. 6G, lanes 3–4, top panel), indicating that CK1 phosphorylation requires phosphorylation at the adjacent PKA sites. In addition, the inactivation of CK1 by the CK1–7 inhibitor blocked the phosphorylation of Smo^{222DSS}, indicating that the phosphorylation was indeed mediated by CK1 (lane 7, top panel).

Phosphorylation at the PKA/CK1 clusters of Smo promotes Cos2 interaction with Smo C-tail

Previous studies have shown that Cos2 binds two distinct domains in the Smo C-terminal tail: one located next to the 7th transmembrane domain and the other in the C-terminus (Jia et al., 2003; Lum et al., 2003). To test whether phosphorylation of Smo at the three clusters promotes the interaction between Smo C-terminus and Cos2, we co-transfected S2 cells with Myc-tagged Smo variants and HA-tagged Cos2 (HA-Cos2) and performed an immunoprecipitation assay to detect the interaction between Smo and Cos2. We found that Smo-Cos2 interaction was enhanced by Hh treatment (Fig. 7A, lanes 1 and 2, top panel) and that the Smo phosphomimetic mutation (Smo^{DDD}) strongly interacted with Cos2 compared to Smo^{WT} (Fig. 7A, lanes 3 and 4, top panel). These results were consistent with the finding that phosphomimetic Smo mutations increased the FRET with Cos2 (Shi et al., 2011). We further found that Smo^{DDA} had a very weak interaction with Cos2 even in the presence of Hh (Fig. 7A, lanes 5 and 6, top panel), suggesting that a phospho-deficient mutation at the third cluster of Smo prevents its interaction with Cos2. Our findings that Smo^{DDA} had very low efficiency of FRET at its C-terminus (Fig. 4T), and that Smo^{DDA} had very low signaling activity *in vivo* (Fig. 4L), suggest that phosphorylation of Smo at

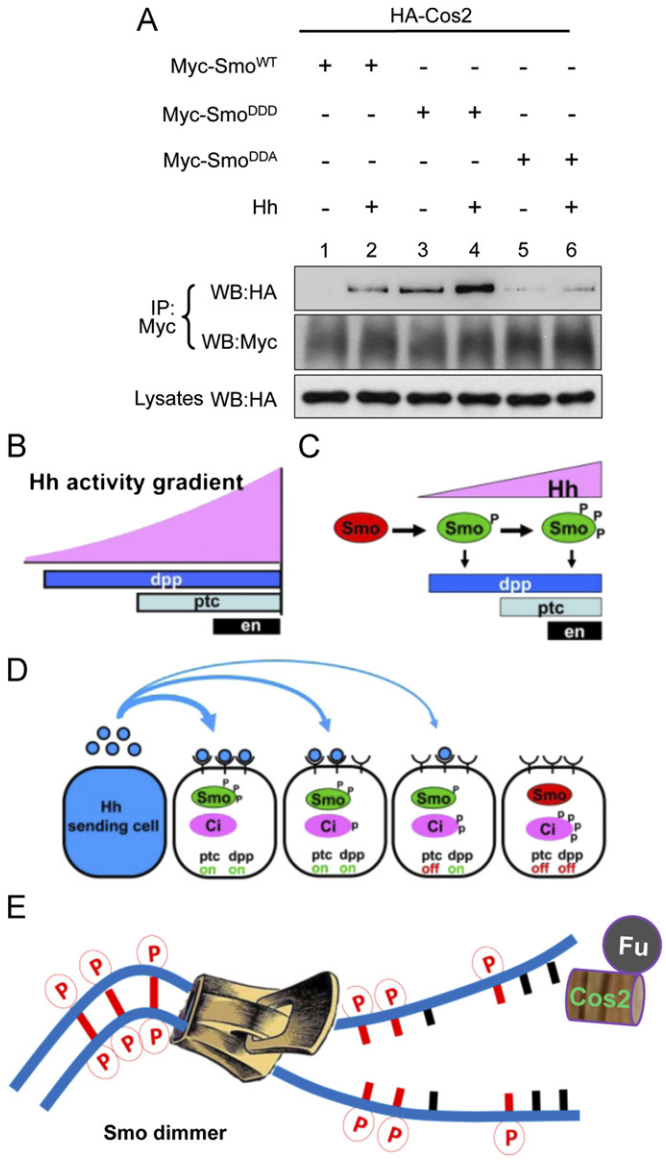

Fig. 7. Mechanisms of Smo phosphorylation and dimerization at the C-terminus. (A) S2 cells were co-transfected with HA-Cos2 and Smo variants. Immunoprecipitation was carried out with anti-Myc antibody followed by western blot with anti-Myc to detect the expression of Smo and anti-HA antibody to detect the bound Cos2. Myc-Smo was normalized by the method described above. Cell lysates were also subjected to direct western blot with the anti-HA antibody to examine the expression of Cos2. (B–D) A model of Smo differential phosphorylation that mediates thresholds of Hh signaling activity: Gene expression pattern in response to Hh activity gradient (B); Increasing Hh activity elevates the levels of Smo phosphorylation (C); Gradient Hh activity signal transduction by differential Smo phosphorylation (D). (E) A zipper-lock model demonstrates the intra-molecular mechanism of the Smo conformational change that is regulated by Hh. Dimerization of the Smo C-terminal tail promotes Cos2 binding.

the three clusters induces a zipper-lock-like dimerization of Smo at its C-terminus, which is responsible for the Hh-induced interaction between Smo and Cos2.

Taken together, these data provide direct evidence that an Hh activity gradient induces differential phosphorylation of Smo, which consequently induces different levels of Hh target gene expression (Fig. 7B–D). Furthermore, we demonstrated that Hh regulates the intra-molecular changes of Smo, which mediates differential Smo cell surface accumulation, dimerization, and activation (Fig. 7E).

Discussion

Smo is a major therapeutic target since it plays a central role in the Hh signaling pathway, and abnormal Smo activation has been shown to play a direct role in basal cell carcinoma and medulloblastoma (Jiang and Hui, 2008). Therefore, understanding the molecular mechanisms underlying Smo activation is currently of great interest in the field. In this study, we show that different levels of Hh signaling activity induce distinct levels of Smo phosphorylation, which promote different levels of Smo cell surface accumulation. By using a phospho-specific antibody, we were able to precisely correlate the levels of signaling activity with the levels of Smo phosphorylation. By carrying out a series of mutagenesis analyses within three phosphorylation clusters, we found that Smo phosphorylation has a positional effect in regulating its activity. Phosphorylation at the first cluster is more critical for triggering Smo activation. In addition, we demonstrated that a phospho-deficient mutation in the third cluster severely blocks dimerization of the C-terminal tail. Therefore, we have provided evidence that thresholds of Hh activity promote differential Smo phosphorylation, which mediates a zipper-lock-like gradual dimerization through three phosphorylation clusters. Since vertebrate Smo is phosphorylated in response to Shh (Chen et al., 2011), the mechanism that we have uncovered here is likely to be conserved in other species.

The contribution of differential phosphorylation to Smo activation

It has been previously shown that Smo is hyperphosphorylated by multiple kinases in response to Hh stimulation (Apionishev et al., 2005; Chen et al., 2010; Jia et al., 2010, 2004; Zhang et al., 2004). Among these kinases, PKA and CK1 are *bona fide* Smo kinases that are essential and responsible for the initiation of Smo phosphorylation by other kinases. Several lines of evidence support this model. First, Smo phosphorylation by PKA and CK1 promotes phosphorylation by GRK2 (Chen et al., 2010). Second, Smo^{DDD}, which is a mutant that contains phosphomimetic mutations at the three clusters, induces the peak level of Hh signaling activity (Jia et al., 2004). Third, using a phospho-specific antibody to detect phosphorylation at the 2nd cluster, we demonstrated that Hh promotes differential phosphorylation of Smo at these clusters, which solely dictates the thresholds of Hh activity. Our findings suggest that a higher stoichiometry of Smo phosphorylation at PKA and CK1 sites promotes higher levels of intermolecular dimerization/oligomerization, and as a result enhances the downstream signaling. It will be interesting to determine the contribution of phosphorylation at other residues, which are not PKA and CK1 sites, to the stoichiometric Smo phosphorylation, as it has been shown that Hh induces phosphorylation at 26 residues located in the Smo C-terminal tail (Zhang et al., 2004). It will be also interesting to examine whether differential phosphorylation of Cos2 (Ranieri et al., 2012) correlates with the differential phosphorylation of Smo.

The regulation of Hh-induced phosphorylation of Smo

In this study, we showed that Hh regulates Smo not only at the inter-molecular but also intra-molecular level. We provide evidence that multiple phosphorylation motifs (clusters) function cooperatively to transduce the Hh signal. Progressive inactivation of these phosphorylation motifs by phospho-deficient mutations incrementally reduces the ability of Smo to promote Hh signaling, whereas activation of these motifs by phosphomimetic mutations enhances this ability. However, a phospho-deficient mutation at a single PKA site among the three clusters (Smo^{ASS}, Smo^{SAS}, and Smo^{SSA} in this study; and Smo^{-PKA1}, Smo^{-PKA2}, and Smo^{-PKA3} in

our previous studies) was not sufficient for impairing the ability of Smo to transduce the Hh signal (this study) (Jia et al., 2004). Smo may employ a "self-correction" mechanism in which phosphorylation at one PKA/CK1 cluster counteracts the deficiency of phosphorylation at the other PKA/CK1 cluster(s). In support of this hypothesis, a phosphomimetic mutation in the background of S > A mutations (Smo^{ADA} and Smo^{DAA}) attenuated the dominant-negative activity of these double mutants (Figs. 5D and E, F and G). It is also possible that phosphorylation at sites outside the three PKA/CK1 clusters could compensate for the reduction in PKA/CK1 phosphorylation at the three clusters.

In this study, we carefully examined the contribution of PKA and CK1 phosphorylation to Smo activation by assessing a series of site mutations. We show that PKA activates Smo by both phosphorylating Smo and priming CK1 phosphorylation of Smo. We found that $SmoD^{PKA}AA^{CK1}$ has a low level of signaling activity by restoring *dpp-lacZ* expression in *smo* mutant cells, and that Smo $A^{PKA}DD^{CK1}$ has lower signaling activity compared to Smo^{DDD} (summarized in Fig. 4A). These observations are consistent with the model in which low levels of Hh induce PKA site phosphorylation, and high levels of Hh induce further phosphorylation by CK1 (Su et al., 2011).

It remains unclear how Hh regulates Smo phosphorylation. It is unlikely that Hh induces Smo phosphorylation by increasing cAMP-dependent PKA activity. For instance, expressing the cAMP-independent PKA catalytic subunit (MC*) in wing discs only caused an anterior expansion of Smo accumulation near the A/P boundary, but did not cause Smo accumulation in A compartment cells away from the A/P boundary where Hh was absent (Jia et al., 2004; Liu et al., 2007). In addition, MC* can substitute for endogenous PKA to confer normal regulation of the Hh pathway (Jiang and Struhl, 1995; Ohlmeyer and Kalderon, 1997), suggesting that Hh does not regulate PKA activity *per se*. However, it is possible that Hh regulates the accessibility of kinases or the phosphatase(s) to Smo, which consequently promotes the hyperphosphorylation of Smo.

Experimental procedures

Constructs, mutants, and transgenes

The creation of the attB-UAST-Myc-Smo^{WT} construct and the generation of transgenes at 75B1 attP locus (resulting VK5 lines) by PhiC31 integration have been previously described (Jia et al., 2009). Smo variants with mutations in the PKA and CK1 sites were generated by site-directed mutagenesis and their transgenes were generated at the 75B1 attP locus, resulting in a series of VK5 lines. Some of the Smo mutants were swapped from constructs generated from our previous studies (Jia et al., 2010, 2004). The approach of making *tub-*Smo^{222} and *UAS-Myc-*Smo^{222} was similar to that of making *tub-*Smo^{WT} previously described (Jia et al., 2010). All of the Smo rescue constructs in combination with the *tubulinα* promoter were generated using the same approach and the corresponding VK5 lines were generated. The genotypes for generating *smo* clones were as follows: *smo* clones expressing VK5-Smo variants by the *tubulinα* promoter, *yw hsp-flp/+or Y; smo3 FRT40/hs-GFP FRT40; UAS-VK5-tub-Smo* variants; or by the *MS1096*-Gal4, *yw hsp-flp, MS1096/+or Y*; *smo3 FRT40/hs-GFP FRT40*; *UAS-VK5-Myc-Smo* variants. GST-Smo^{-PKA} and GST-Smo^{-CK1} containing Smo aa656-755 with either the single PKA site or the two CK1 sites in the 2nd cluster mutated to alanine. The *tub*-Ci construct was created by replacing the *UAS* binding sites in *pUAST* with the *tubulinα* promoter and then subsequently fusing the 2HA-Ci cDNA afterward. HA-Cos2 has been previously described (Liu et al., 2007), and flies of *C765*-Gal4, *MS1096* Gal4, and *ap*-Gal4 have been previously described (Flybase) (Jia et al., 2010; Liu et al., 2007).

Anti-SmoP antibody production

The anti-SmoP antibody was generated by Genemed Synthesis Inc. by injecting the antigen peptide CRHVSVESRRN(pS)VD(pS)QV(pS)VK into rabbits. The serum was affinity-purified with the antigen and the flowthrough was kept as a control antibody against non-phosphorylated peptide.

In vitro kinase assay

For the *in vitro* kinase assay, GST-Smo fusion proteins were expressed in bacteria, purified with standard protocols, and subjected to a kinase assay with commercial PKA and CK1 (New England Biolabs) according to the supplier's protocols. Phosphorylated proteins were then analyzed by western blot with either anti-GST or anti-SmoP antibodies.

Cell culture, transfection, immunoprecipitation, western blot, and luciferase reporter assay

S2 cells were cultured as previously described (Liu et al., 2007). The transfection was carried out using Effectene transfection reagent (Qiagen). The immunoprecipitation and immunoblot analysis were performed using a standard protocol. The use of HhN-conditioned medium has been previously described (Liu et al., 2007). Treating S2 cells with H-89 and CK1–7 inhibitors has also been previously described (Jia et al., 2004). The method of using MG132 (Calbiochem), a proteasome inhibitor, and NH4Cl (Sigma-Aldrich), a lysosome inhibitor, to block Smo degradation has been previously described (Li et al., 2012; Xia et al., 2012). Antibodies used in this study were as follows: mouse anti-Myc (9E10, Santa Cruz, 1:5000), anti-Flag (M2, Sigma, 1:10000), anti-HA (F7, Santa Cruz, 1:1500), anti-GFP (Millipore, 1:1000); rabbit anti-SmoP (this study, 1:50), anti-PKA (Santa Cruz, 1:5000), and anti-GST (Santa Cruz, 1:10000). For *ptc-luciferase* reporter assays, S2 cells were cultured in 6-well plates and transfected with 50 ng *tub*-Ci and 150 ng *ptc-luciferase* reporter constructs with or without Smo variant constructs. After 48 h post-transfection, the cells were lysed for luciferase activity analysis using the Dual-Luciferase Reporter Assay System (Promega, Madison, WI, USA). Renilla was used to normalize the luciferase activity. The measurements of Dual-Luciferase were performed using a GLOMAX Multi Detection System (Promega). A representative assay of three is shown and error bars indicate standard deviation (S.D.) from four repeats.

Cell surface staining and FRET analysis using confocal microscopy

The cell-based assay to detect Smo cell surface accumulation was carried out by immunostaining with the anti-SmoN antibody before cell permeabilization (Jia et al., 2004). For FRET analysis, S2 cells transfected with Smo constructs tagged with CFP or YFP at the C-terminus were treated with HhN-conditioned medium or control medium. For maximal Hh signal strength, a UAST-Hh construct was also included in the transfection. Cells were then washed with PBS, fixed with 4% formaldehyde for 20 min, and mounted on slides in 80% glycerol. Fluorescence signals were acquired with the 60 x objective on an Olympus confocal microscope. CFP was excited at 458nm wavelength and the emission was collected through a BA 480–495 nm filter. YFP was excited at 514 nm wavelength and the emission was collected through a BA 535–565 nm filter. The CFP signal was obtained once before (BP) and once after (AP) photobleaching YFP using the full power of the 515 nm laser line for 2–3 min at the top half of each cell, leaving the bottom half of the cell as an internal control.

The intensity change of CFP was analyzed using the Olympus Fluoview software. The efficiency of FRET was calculated using the formula: $FRET\% = [(CFP_{AP} - CFP_{BP})/CFP_{AP}] \times 100\%$. Each data set was based on 15 individual cells. In each cell, five regions of interest in the photobleached area were selected for analysis.

Immunostaining of wing imaginal discs

A standard protocol was used for the wing disc immunostaining assay. Antibodies used in this study were as follows: mouse anti-Myc (9E10, Santa Cruz, 1:50), anti-Flag (M2, Sigma, 1:150), anti-SmoN (DSHB, 1:10), anti-Ptc (DSHB, 1:10), anti-En (DSHB, 1:20); rabbit anti-SmoP (this study, 1:10), anti-β-Gal (Cappel, 1:1500), anti-GFP (Clontech, 1:500), anti-PKA (Santa Cruz, 1:150); and rat anti-Ci, 2A1 (Motzny and Holmgren, 1995).

Acknowledgments

This project was initiated in Dr. Jin Jiang's laboratory years ago and we are grateful to Dr. Jiang for helpful discussions. We thank Mary K. Brewer for technical assistance. We thank the Developmental Studies Hybridoma Bank (DSHB) for antibodies. This study was supported by grants from the National Institutes of Health (GM079684) and the American Heart Association (0830009N) to J. Jia.

Appendix A. Supporting information

Supplementary data associated with this article can be found in the online version at http://dx.doi.org/10.1016/j.ydbio.2012.04.007.

References

Aikin, R.A., Ayers, K.L., Therond, P.P., 2008. The role of kinases in the Hedgehog signalling pathway. EMBO Rep. 9, 330–336.
Apionishev, S., Katanayeva, N.M., Marks, S.A., Kalderon, D., Tomlinson, A., 2005. Drosophila Smoothened phosphorylation sites essential for Hedgehog signal transduction. Nat. Cell Biol. 7, 86–92.
Basler, K., Struhl, G., 1994. Compartment boundaries and the control of Drosophila limb pattern by hedgehog protein. Nature 368, 208–214.
Bischof, J., Maeda, R.K., Hediger, M., Karch, F., Basler, K., 2007. An optimized transgenesis system for Drosophila using germ-line-specific phiC31 integrases. Proc. Nat. Acad. Sci. USA 104, 3312–3317.
Campbell, G., Tomlinson, A., 1999. Transducing the Dpp morphogen gradient in the wing of Drosophila: regulation of Dpp targets by brinker. Cell 96, 553–562.
Chen, Y., Li, S., Tong, C., Zhao, Y., Wang, B., Liu, Y., Jia, J., Jiang, J., 2010. G protein-coupled receptor kinase 2 promotes high-level Hedgehog signaling by regulating the active state of Smo through kinase-dependent and kinase-independent mechanisms in Drosophila. Genes Dev. 24, 2054–2067.
Chen, Y., Sasai, N., Ma, G., Yue, T., Jia, J., Briscoe, J., Jiang, J., 2011. Sonic Hedgehog dependent phosphorylation by CK1alpha and GRK2 is required for ciliary accumulation and activation of smoothened. PLoS Biol. 9, 1001083. e.
Denef, N., Neubuser, D., Perez, L., Cohen, S.M., 2000. Hedgehog induces opposite changes in turnover and subcellular localization of patched and smoothened. Cell 102, 521–531.
Hooper, J.E., Scott, M.P., 2005. Communicating with Hedgehogs. Nat. Rev. Mol. Cell Biol. 6, 306–317.
Ingham, P.W., McMahon, A.P., 2001. Hedgehog signaling in animal development: paradigms and principles. Genes Dev. 15, 3059–3087.
Ingham, P.W., Nakano, Y., Seger, C., 2011. Mechanisms and functions of Hedgehog signalling across the metazoa. Nat. Rev. Genet. 12, 393–406.
Jia, H., Liu, Y., Xia, R., Tong, C., Yue, T., Jiang, J., Jia, J., 2010. Casein kinase 2 promotes Hedgehog signaling by regulating both smoothened and Cubitus interruptus. J. Biol. Chem. 285, 37218–37226.
Jia, H., Liu, Y., Yan, W., Jia, J., 2009. PP4 and PP2A regulate Hedgehog signaling by controlling Smo and Ci phosphorylation. Development 136, 307–316.
Jia, J., Jiang, J., 2006. Decoding the Hedgehog signal in animal development. Cell Mol. Life Sci. 63, 1249–1265.
Jia, J., Tong, C., Jiang, J., 2003. Smoothened transduces Hedgehog signal by physically interacting with Costal2/Fused complex through its C-terminal tail. Genes Dev. 17, 2709–2720.
Jia, J., Tong, C., Wang, B., Luo, L., Jiang, J., 2004. Hedgehog signalling activity of Smoothened requires phosphorylation by protein kinase A and casein kinase I. Nature 432, 1045–1050.
Jiang, J., Hui, C.C., 2008. Hedgehog signaling in development and cancer. Dev. Cell 15, 801–812.
Jiang, J., Struhl, G., 1995. Protein kinase A and hedgehog signaling in Drosophila limb development. Cell 80, 563–572.
Lecuit, T., Brook, W.J., Ng, M., Callega, M., Sun, H., Cohen, S.M., 1996. Two distinct mechanisms for long-range patterning by Decapentaplegic in the Drosophila wing. Nature 381, 387–393.
Li, S., Chen, Y., Shi, Q., Yue, T., Wang, B., Jiang, J., 2012. Hedgehog-regulated ubiquitination controls smoothened trafficking and cell surface expression in Drosophila. PLoS biology 10, e1001239.
Liu, Y., Cao, X., Jiang, J., Jia, J., 2007. Fused Costal2 protein complex regulates Hedgehog-induced Smo phosphorylation and cell-surface accumulation. Genes Dev. 21, 1949–1963.
Lum, L., Beachy, P.A., 2004. The Hedgehog response network: sensors, switches, and routers. Science 304, 1755–1759.
Lum, L., Zhang, C., Oh, S., Mann, R.K., von Kessler, D.P., Taipale, J., Weis-Garcia, F., Gong, R., Wang, B., Beachy, P.A., 2003. Hedgehog signal transduction via Smoothened association with a cytoplasmic complex scaffolded by the atypical kinesin, Costal-2. Mol. Cell 12, 1261–1274.
Motzny, C.K., Holmgren, R., 1995. The Drosophila cubitus interruptus protein and its role in the wingless and hedgehog signal transduction pathways. Mec. Dev. 52, 137–150.
Nellen, D., Burke, R., Struhl, G., Basler, K., 1996. Direct and Long-Range Action of a DPP Morphogen Gradient. Cell 85, 357–368.
Ogden, S.K., Ascano Jr., M., Stegman, M.A., Suber, L.M., Hooper, J.E., Robbins, D.J., 2003. Identification of a functional interaction between the transmembrane protein Smoothened and the kinesin-related protein Costal2. Curr. Biol. 13, 1998–2003.
Ohlmeyer, J.T., Kalderon, D., 1997. Dual pathways for induction of wingless expression by protein kinase A and Hedgehog in Drosophila embryos. Genes Dev. 11, 2250–2258.
Ranieri, N., Ruel, L., Gallet, A., Raisin, S., Therond, P.P., 2012. Distinct phosphorylations on Kinesin costal-2 mediate differential hedgehog signaling strength. Dev. Cell 22, 279–294.
Riddle, R.D., Johnson, R.L., Laufer, E., Tabin, C., 1993. Sonic hedgehog mediates the polarizing activity of the ZPA. Cell 75, 1401–1416.
Roelink, H., Porter, J.A., Chiang, C., Tanabe, Y., Chang, D.T., Beachy, P.A., Jessell, T.M., 1995. Floor plate and motor neuron induction by different concentrations of the amino-terminal cleavage product of sonic hedgehog autoproteolysis. Cell 81, 445–455.
Shi, Q., Li, S., Jia, J., Jiang, J., 2011. The Hedgehog-induced Smoothened conformational switch assembles a signaling complex that activates Fused by promoting its dimerization and phosphorylation. Development, 4219–4231.
Strigini, M., Cohen, S.M., 1997. A Hedgehog activity gradient contributes to AP axial patterning of the Drosophila wing. Development 124, 4697–4705.
Su, Y., Ospina, J.K., Zhang, J., Michelson, A.P., Schoen, A.M., Zhu, A.J., 2011. Sequential phosphorylation of smoothened transduces graded hedgehog signaling. Sci. Signal. 4, ra43.
Tabata, T., Kornberg, T.B., 1994. Hedgehog is a signaling protein with a key role in patterning Drosophila imaginal discs. Cell 76, 89–102.
Venken, K.J., He, Y., Hoskins, R.A., Bellen, H.J., 2006. P[acman]: a BAC transgenic platform for targeted insertion of large DNA fragments in D. melanogaster. Science 314, 1747–1751.
Vervoort, M., Crozatier, M., Valle, D., Vincent, A., 1999. The COE transcription factor Collier is a mediator of short-range Hedgehog-induced patterning of the Drosophila wing. Curr. Biol. 9, 632–639.
Xia, R., Jia, H., Fan, J., Liu, Y., Jia, J., 2012. USP8 Promotes Smoothened Signaling by Preventing Its Ubiquitination and Changing Its Subcellular Localization. PLoS Biology 10, e1001238.
Zhang, C., Williams, E.H., Guo, Y., Lum, L., Beachy, P.A., 2004. Extensive phosphorylation of Smoothened in Hedgehog pathway activation. Proc. Nat.Acad. Sci. USA 101, 17900–17907.
Zhao, Y., Tong, C., Jiang, J., 2007. Hedgehog regulates smoothened activity by inducing a conformational switch. Nature 450, 252–258.
Zheng, X., Mann, R.K., Sever, N., Beachy, P.A., 2010. Genetic and biochemical definition of the Hedgehog receptor. Genes Dev. 24, 57–71.